Clusterization aspects in the states of non-rotating and fast rotating nuclei

A.V. Afanasjev[1,*]

[1]Department of Physics and Astronomy, Mississippi State University, MS 39762

Abstract. The understanding of clustering aspects at the ground state of nuclei and in fast rotating ones within the framework of covariant density functional theory has been reviewed and reanalyzed. The appearance of many exotic nuclear shapes in nuclear chart can be inferred from combined analysis of nodal structure of the densities of the single-particle states and the evolution of such states in the Nilsson diagram with deformation and particle number. Such analysis which is supported by fully self-consistent calculations allows to predict the existence of nuclear configurations with specific shape or cluster properties at ground state and at high spin. For example, it indicates that in a given shell with principal quantum number N only the lowest in energy two-fold degenerate deformed state can contribute to the formation of linear chain α cluster structures.

1 Introduction

For a long time light nuclei have been a playground for nuclear physicists to study the existence and coexistence of different types of nuclear shapes such as α-clustered, nuclear molecules, the combination of large spheroidal-like cluster and α-particles, ellipsoidal like ones etc (see, for example, Refs. [1, 2]). Among recent interesting results is the experimental observation of rotational band in ^{14}C which is built on linear chain of three α-particles plus two neutrons (see Ref. [3]) and theoretical investigation of the α clusterization in the ^{8}Be and ^{12}C nuclei in ab-initio calculations (see Ref. [4]).

Above mentioned shapes have been analysed in the framework of different theoretical models. One class of such models is the cluster models. It provides an important insight into cluster dynamics of nucleus but is not able to describe many shell model configurations and is limited by model assumptions. Alternatively, the formation of the clusters and other exotic shapes via microscopic single-nucleon degrees of freedom and many-body correlations can be described in density functional theory (DFT) (see Refs. [1, 5–12]).

In the present paper, I review and reanalyze the results obtained in the framework of cranked relativistic mean field theory in Refs. [10–12] and present some new results. Note that in this paper we restrict our consideration to reflection-symmetric shapes characterized by extreme deformation. A particular attention is paid to the correlations between nodal structure of the density distributions of the single-particle states and the creation of exotic shapes as a function of particle number and deformations. The impact of collective rotation on these features is also analyzed.

*e-mail: Anatoli.Afanasjev@gmail.com

2 Nodal structure of the wavefunctions of occupied single-particle states: a key to understanding the clusterization and nuclear molecules in finite nuclei

The phenomenon of clusterization in finite nuclei is intimately connected with the nodal structure of the wavefunctions and densities of occupied single-particle states. To better understand its role let me start from the analysis of the single-particle densities at spherical shape. The single-particle densities of the s states have a maximum at radial coordinate $r = 0$ (see Fig. 1(a)). This is because their orbital angular momentum is $l = 0$ and thus there is no centrifugal barrier. Dependent on principal quantum number n their densities look like a sphere of variable density with maximum density at center (see the $n = 1$ curve in Fig. 1(a)) or as a combination of similar sphere and a spherical shell(s)[1] of variable density: the maximum of the density of the shell is located at R (see the $n = 2$ curve in Fig. 1(a)). The measurements of the single-particle densities of the $3s$ state in spherical nuclei near ^{208}Pb confirm this picture (see Ref. [13, 14]).

In contrast no density can be built at $r = 0$ for the single-particle states which have orbital momentum $l \neq 0$ (i.e. the p^2, d, f, g ... single-particle states) due to the presence of centrifugal barrier. The densities of the single-particle states can be viewed as a combination of n spherical shells the maxima of the density of which appear at the R_i radial coordinates (see Fig. 1(b)). In both cases the number of independent structures (sphere and/or spherical shells) is equal to principal quantum number n and the node(s) of the single-particle wave functions at

[1]In geometry, a spherical shell is a region between two concentric spheres of differing radii.

[2]Note that in relativistic framework the p states have some part of small component of the Dirac spinor in the s states which build the density at $r = 0$, see Sec. IV of Ref. [15].

which $\rho = 0$ define the natural boundary between these these structures (see Ref. [16]). Note that the nodal structure of the wavefunctions and densities of spherical single-particle states plays very important role in our understanding of the formation of bubble structures in the nuclei (see Ref. [15]) and the buildup of differential charge radii as a function of neutron number in isotopic chains (see Ref. [16]).

The situation is drastically different for extremely deformed structures such as hyper- and megadeformed ones. In some instances such structures are denoted as rod-shaped (see Refs. [11, 17]). For such shapes, the single-particle states are characterized by asymptotic quantum numbers $[Nn_z\Lambda]\Omega$ (Nilsson quantum numbers) of the dominant component of the wave function. Their wave functions $\Psi_{[Nn_z\Lambda]\Omega}$ are expanded into the basis states $|N'n'_z\Lambda'\Omega' >$ by

$$\Psi_{[Nn_z\Lambda]\Omega} = \sum_{N',n'_z,\Lambda',\Omega'} c_{N'n'_z\Lambda'\Omega'}|N'n'_z\Lambda'\Omega' > . \qquad (1)$$

Here, the basis states are characterized by principal quantum number N', the number n'_z of nodes in the axial direction (z-direction) and the projections of orbital (Λ') and total (Ω') single-particle angular momenta on the axis of symmetry. The sum in Eq. (1) runs over all allowable combinations of the quantum numbers N', n'_z, Λ' and Ω'.

In the context of the discussion of clusterization it is important that the single-particle wavefunctions at extremely large deformation are dominated by a single basis state. This is the case for the configurations of interest of light nuclei (see Ref. [11]). This basis state defines the dominant nodal structure of the wave function of the single-particle state and its spatial density distribution. It turns out that only two types of the states i.e. $|N, n_z, \Lambda \rangle = |N, N, 0 \rangle$ [3] and $|N, n_z, \Lambda \rangle = |N, N-1, 1 \rangle$ are important for the nuclei with masses $A \leq 50$ (see Ref. [11]). The density distribution of the basis states with the $|NN0 \rangle$ structure is axially symmetric. It consist of the $N+1$ clusters the maxima of the density of which are located at the axis of symmetry. In contrast, the density distribution of the basis states with the $|N, N-1, 1 \rangle$ structure is build of the N donuts (or ring-like structures) the axis of the symmetry of which coincides with the axis of symmetry of the nucleus. Note that the nodal structure of the density distribution of the basis state is defined by the condition $N' = n'_z + 2n'_r + |\Lambda'|$ where n'_r is the number of radial nodes. In the light nuclei, the basis states of interest have $n'_r = 0$, so above mentioned condition is simplified to $N' = n'_z + |\Lambda'|$.

Fig. 1 illustrates this situation. Let me first consider the states with the $|NN0 >$ structure at extreme deformation. The $[0, 0, 0]1/2$ deformed state emerges from the spherical $1s_{1/2}$ state (see Fig. 2) which has orbital angular momentum $l = 0$. Because of the latter fact extreme deformation $\beta_2 \sim 1.6$ leads only to the elongation of its single-particle density [see Fig. 1(c)]. The lowest in energy extremely deformed state of the $N = 1$ shell (i.e. the $[110]1/2$ state) emerges from the spherical $1p_{3/2}$ state (see Fig. 2) which has $l = 1$. Its single-particle density is formed of two clusters separated by the gap [see Fig. 1(e)]. The $[220]1/2$ extremely deformed state emerges from the lowest state of the $N = 2$ shell (i.e. the $1d_{3/2}$ one): its density consist of three clusters [see Fig. 1(d)].

The nodal structure of the density distribution of single-particle states in spherical nuclei is defined by the principal quantum number n. In contrast, it is defined by the n_z value of the Nilsson label of the single-particle state in extremely deformed nuclei: the number of density clusters along the symmetry axis is equal to n_z+1 in the single-particle states with the $|NN0 >$ structure. That means that the memory of the nodal structure of the density distribution of single-particle state at spherical shape is completely lost on transition to extremely deformed shapes. Note that this result is also confirmed by the analysis of the $[330]1/2$, $[440]1/2$ and $[550]1/2$ single-particle states in the light nuclei (see Figs. 4 and 9 in Ref. [11] and Fig. 8 in supplemental material to Ref. [11]) and in the $[770]1/2$ state of yrast superdeformed band of ^{152}Dy (see Fig. 9(a) in Ref. [20]).

Doughnut-like structures of the single-particle density distribution at extreme deformation is illustrated by the example of the $[101]3/2$ and $[211]3/2$ states [see Figs. 1(f) and(g)]. The first state emerges from the $1p_{3/2}$ spherical subshell (see Fig. 2) and its single-particle density has single dooughnut structure. The second one originates from the $2d_{3/2}$ spherical subshell (see Fig. 2): its single-particle density looks like two doughnuts located symmetrically with respect of the center of the nucleus. Higher number of donuts in the single-particle density is also possible (see, for example, Fig. 8 in Ref. [11]).

The wave functions of normal deformed nuclei with quadrupole deformation $\beta_2 \approx 0.3$ are dominated by few spherical components. This is because the shapes of such nuclei do not deviate substantially from spherical ones. Thus, the densities of the single-particle states at such deformations are the mixtures of the densities shown in left panels of Fig. 1 and the formation of well separated clusters or donuts seen at extreme deformation does not take place at normal deformation. As a result, one can conclude that the clusterization features do not appear in the single-particle structures at spherical and normal deformed shapes in finite nuclei.

The Nilsson diagram for the states of interest is shown in Fig. 2. The single-particle states for which detailed analysis of the nodal structure of the density distribution has been carried out in the present paper and in Ref. [11] are shown by thick lines of different color. The states for which no such analysis is available are shown by thin blue lines but they do not play a role in the configurations of interest in the $A \leq 50$ nuclei. At extreme deformation, all the states shown by thick lines can be separated into three classes:

- *cluster forming states* i.e. the single-particle states dominated by the $|N, N, 0 \rangle$ basis state which leads to a formation of the $N+1$ spheroidal-like density clusters along

[3] The nodal structure of the single-particle wave function and thus of its density distribution is defined by the spatial part of the wave function. Thus, at no rotation it is sufficient to specify only Λ and to drop Ω.

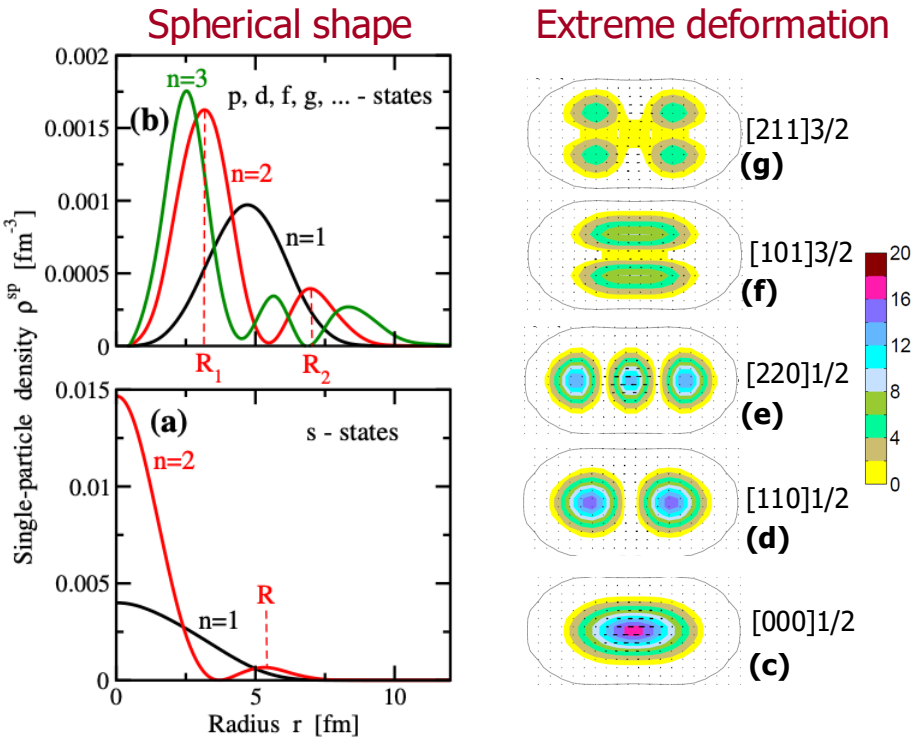

Figure 1. Left panels: schematic illustration of the nodal structure of density for different single-particle states at spherical shape (see Refs. [15, 16] for more detailed information). Right panels: the pattern of nodal structure of the density of the single-particle states at extreme deformation (for analysis of three-dimensional density distributions see Ref. [11]). The neutron densities are plotted for indicated Nilsson states in ^{40}Ca at deformation $\beta_2 \approx 1.6$ which roughly corresponds to megadeformed configurations in this nucleus. The shape of the nucleus is shown by black solid line. The colormap shows densities as multiplies of 0.001 fm^{-3}. The plotting of the densities starts from 0.001 fm^{-3}.

the axis of symmetry of the nucleus. These states are shown by red thick lines in Fig. 2.

- *single doughnut states* i.e. the single-particle states which are dominated by the $|N, 0, 1\rangle$ basis state the density distribution of which is represented by a single doughnut. They are shown by green thick lines in Fig. 2.

- *multiply doughnut states* i.e. the single-particle states the density of which is defined by the $|N, N-1, 1\rangle$ ($N \geq 2$) basis state which contains N doughnuts. They are shown by black thick lines in Fig. 2.

The present analysis of the nodal structure of the single-particle densities at extreme deformation indicates that linear α-chain structures (such as those shown in Fig. 1 of Ref. [21] and Fig. 4 of Ref. [8]) can only be formed by the occupation of cluster forming states. These are 2α, 3α, 4α, and 5α linear-chain structures in ^{8}Be, ^{12}C, ^{16}O and ^{20}Ne nuclei, respectively. The present analysis for the first time reveals that there is only one two-fold degenerate deformed single-particle state in a given N-shell which acts as α-cluster forming state. These are the lowest in energy states in a given N-shell shown by red thick lines in Fig. 2. Note that above mentioned multiply α-cluster structures are located at very high excitation energies with respect of the ground states of the nuclei under discussion.

The occupation of single and/or multiply dooughnut states will lead to suppression of the α-clusterization and formation of ellipsoidal and nuclear molecule shapes. The analysis of the nodal structure of the single-particle densities at extreme deformation (see Fig. 1) and Nilsson diagram (see Fig. 2) leads to conclusion that only for a very few specific nucleonic configurations the processes of formation of the α-cluster structures is possible. There are several reasons for that. First, the portion of cluster forming single-particle states in a given N shell drastically decreases with increasing principal quantum number N: such states represent only 100%, 33%, 15%, 10%, and 6.5% of all single-particle states in the $N = 0$, 1, 2, 3 and 4 shells, respectively. Second, because of the rarity of cluster forming single-particle states this process is possible only in relatively light nuclei since with increasing proton and neutron numbers the process of the occupation of single and/or multiply doughnut states becomes inevitable (see Fig. 2). Third, with increasing particle number the contribution of the states favoring α-clusterization into the structure of total wavefunction decreases and ellipsoidal-like shapes become dominant species of nuclear shapes.

Considering typical pattern of density distributions of single-particle states presented in right panels of Fig. 1 and the arrangement of the single-particle states at extreme deformation (see Fig. 2) one can easily predict the existence of exotic structures which are built from large cen-

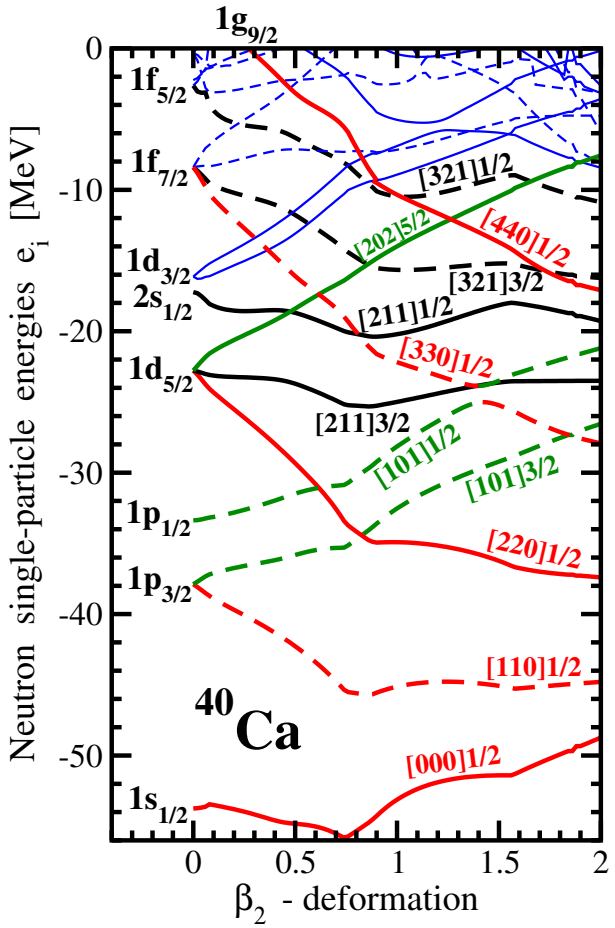

Figure 2. The energies of the single-particle states in ^{40}Ca as a function of quadrupole deformation β_2. They are calculated along the deformation path of the lowest in total energy solution in axial relativistic Hartree-Bogoliubov framework [18] using the NL3* CEDF [19]. The orbitals are labelled by means of asymptotic quantum numbers (Nilsson labels) $[Nn_z\Lambda]\Omega$. Solid and dashed lines are used for positive and negative parity states, respectively. Note that in the case of the [330]1/2 and [440]1/2 single-particle states, the structure of these states are traced before and after the crossing of these states with another ones. See text for further details.

tral spheroidal-like structure and two alpha particles on opposite sides of it located at the same axis of symmetry. The examples of density distributions of such exotic structures are shown in Fig. 4 of Ref. [8] (second from bottom density distribution in the ^{20}Ne nucleus and third one in ^{24}Mg). For example, the configuration $confA(^{16}\mathrm{O}) = [000]1/2 \otimes [110]1/2 \otimes [220]1/2 \otimes [101]3/2$[4] in ^{16}O is an example of such exotic structure. The occupation of first three orbitals by protons and neutrons leads to triple linear α chain similar to that which exists in ^{12}C (see Fig. 1(a) in Ref. [11] and Fig. 2 in Ref. [17]). The [101]3/2 orbital has single doughnut structure of single-particle densities [see Fig. 1(f)]: its occupation in combination with central α cluster leads to the formation of central spheroidal-like structure. Note that Fig. 2 suggests that this configuration is the lowest in energy at extreme deformation $\beta_2 = 1.2 \pm 0.4$.

Similar exotic structures can be built starting from $confA(^{16}\mathrm{O})$ in heavier nuclei. For example, the addition of two protons and two neutrons leads to the configurations $confA(^{20}\mathrm{Ne}) = confA(^{16}\mathrm{O}) + [101]1/2$ and $confB(^{20}\mathrm{Ne}) = confA(^{16}\mathrm{O}) + [303]1/2$ in ^{20}Ne (see Fig. 2) which have similar exotic structure. Note that central spheroidal-like structure will be more pronounced in the former configuration since the density of the [101]1/2 state has single doughnut structure (see Fig. 1(f)). Note that the latter configuration is built from linear 4α chain, which is analyzed in the case of ^{16}O in Refs. [9, 22], and the doughnut density distribution generated by the [101]3/2 state. Nilsson diagram of Fig. 1 suggests that $confA(^{20}\mathrm{Ne})$ is more energetically favored as compared with $confB(^{20}\mathrm{Ne})$ at $\beta_2 \leq 1.3$ but the situation becomes reversed at higher deformations. Fig. 2 suggests that the $confA(^{24}\mathrm{Mg}) = [000]1/2 \otimes [110]1/2 \otimes [220]1/2 \otimes [330]1/2 \otimes [101]3/2 \otimes [101]1/2$ configuration in ^{24}Mg should be close to the lowest one at $\beta_2 \geq 1.2$. The occupation of the first four orbitals builds linear 4α chain while the occupation of the last two ones builds single doughnut structure around an axis of symmetry of the nucleus located at its center. Resulting total density is close to the one shown in Fig. 4 of Ref. [8] (third from bottom density distribution in ^{24}Mg). Note that this configuration can be rewritten as $confA(^{24}\mathrm{Mg}) = confA(^{16}\mathrm{O}) \otimes [330]1/2 \otimes [101]1/2$.

The formation of ellipsoidal-like shapes at extreme deformation requires the occupation of all three classes of single-particle states, i.e. cluster forming states, which built density along the axis of symmetry of the nucleus, and single and multiply doughnut states. This process starts when the [211]3/2, [211]1/2, [321]3/2 and [321]1/2 states which have multiply doughnut structure of the single-particle density and which are shown by thick black lines in Fig. 2 start to be occupied in the configurations of interest. To build the nuclear molecules one has to move the matter from the neck (equatorial) region into the polar regions of the nucleus. To achieve that one should remove the particles from the states which have single doughnut structure of the single-particle density (i.e. single-particle states with the $|N, 0, 1\rangle$ structure shown by thick green lines in Fig. 2). Some examples of particle-holes excitations leading to nuclear molecules have been discussed in Ref. [11].

3 The role of rotation in the clusterization of atomic nuclei

Unfortunately, at spin zero the absolute majority of predicted extremely deformed structures cannot be observed in experiment. This is because they are located at very high excitation energies of 15 to 40 MeV and in many cases no local minimum corresponding to such shapes exists in potential energy surfaces (see, for example, Fig. 2 in Ref. [8] and Fig. 1 in Ref. [9]). The collective rotation

[4]For simplicity of discussion we consider here only the $N = Z$ nuclei with $A = 4Z$. Thus, each of single-particle states in the configuration label is occupied by two protons and two neutrons.

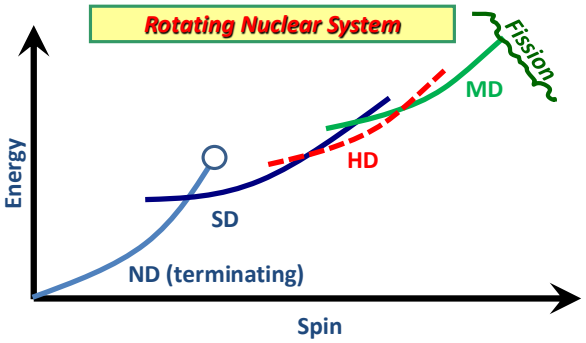

Figure 3. General structure of rotational spectra in light ($A < 50$) nuclei. Based on the results of systematic investigations presented in Refs. [10, 12]. Terminating state of normal deformed band is shown by open circle. See text for further details.

of the nuclei makes the conditions for the observation of extremely deformed structures at high spin more favorable than at low one because of the following reasons:

- The angular momentum of the rotational bands build on the ground state and low excited configurations in the nuclei of interest is quite limited. For example, ground state rotational band of ^{20}Ne terminates at $I = 8^+$ and in some of the nuclei of interest such termination is expected even at lower spins. Thus, above such spins the yrast line is predicted to be formed by the configurations which are built by sequential particle-hole excitations leading to larger angular momentum content and larger deformations of these configurations (see Refs. [10, 12]). This is schematically illustrated in Fig. 3 where along the yrast line with increasing spin normal deformed (ND) configurations are first replaced by superdeformed (SD) ones, then by hyperdeformed (HD) ones and finally by megadeformed (MD) configurations. The experimental spectra of ^{40}Ca confirms this structure and shows the transition from spherical ground state at $I = 0$ to the ND structures at moderate spins and then to the SD rotational band at high spins (see Ref. [23]).
- The rotation leads to the change of the energies of the single-particle states and the emergence of new shell closures (see, for example, Figs. 2-4 in Ref. [10]) which stabilizes respective extremely deformed minima at rotation. Especially important role in this process is played by intruder orbitals emerging from the lowest deformed state of a given N shell (see above mentioned figures). As discussed in Sec. 2, these are cluster forming states which play important role in the formation of linear α cluster structures in light nuclei.
- At the spins of interest static pairing correlations in extremely deformed configurations are substantially quenched by a combination of factors which include Coriolis antipairing effect induced by collective rotation [24, 25], the emergence of large shell gaps [26] and blocking effect induced by particle-hole excitations [24]. This leads to a significant reduction or even suppression of configuration mixing induced by pairing correlations. As a consequence, the structure of total density of nucleonic configurations is defined by the single-particle densities of occupied states and their nodal structure discussed in Sec. 2. In addition, weak or no pairing is expected to lead to a substantial increase of the fission barrier as compared with the case of regular pairing (see Ref. [27]). This will extend the spin range at which rotational states can exist to a higher limit.

On the one hand, the collective rotation leads (via Coriolis interaction) to some reduction of the weight of the dominant basis state in the single-particle wave function and to some delocalization of single-particle density (i.e. to some suppression of both α-clusterization and the formation of nuclear molecules) (see Ref. [11]). However, for the single-particle states located at and near the bottom of nucleonic potential (i.e. for those shown by thick lines in Fig. 2) the rotation preserves the nodal structure of the densities of the single-particle states (see Ref. [11]). On the other hand, collective rotation suppresses pairing interaction and as a consequence the configuration mixing induced by it and brings extremely deformed rotational states to the yrast line. The former feature counteracts some suppression of α-clusterization and the formation of nuclear molecules induced by rotation at the level of the structure of single-particle states. The latter one favors the population of such states in ion collisions which potentially makes experimental observation of extremely deformed states at high spin feasible.

4 New type of cluster structures

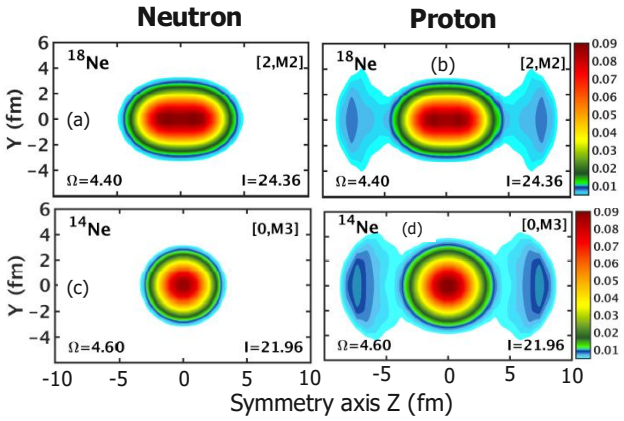

Figure 4. Neutron (left column) and proton (right column) density distributions of the configurations in ^{18}Ne and ^{14}Ne at indicated spins and frequencies. The density colormap starts at $\rho = 0.005$ fm^{-3} and shows the densities in fm^{-3}. The results for ^{14}Ne are taken from Ref. [12]. For details of configuration labelling see Sec. 5.2.2 in Ref. [12].

As discussed above, the lowest in energy deformed states emerging from each N shell have the $[NN0]1/2$ structure. These states are the only ones which lead to the α clusterization. One can see that with increasing deformation such states shown by thick red lines in Fig. 2 come close to each other. This explains why linear chain $n\alpha$ cluster configurations such as $[000]1/2 \otimes [110]1/2$ in

^{8}Be, [000]1/2⊗[110]1/2⊗[220]1/2 in ^{12}C and [000]1/2⊗[110]1/2⊗[220]1/2⊗[330]1/2 in ^{16}O appear as the lowest in energy at extreme deformations.

There are two peculiar features about the $[NN0]1/2$ single-particle states. First, in the single-particle densities the maxima of the density of the clusters located farthest away (in polar region) from the center of nucleus are substantially higher than those for the clusters located at or near the center of the nucleus. This feature is especially pronounced for $N \geq 3$ (see Figs. 4 and 9 in Ref. [11], Fig. 8 in supplemental material to Ref. [11]) and Fig. 9(a) in Ref. [20]). Second, the lowest in energy signature branch of such states has the largest single-particle angular momentum alignment in a given N shell. Because of this feature such states are strongly down-sloping as a function of rotational frequency Ω_x (see, for example, the evolution of the $[440]1/2(r = -i)$ orbital in Figs. 2, 3 and 4 in Ref. [10]). As a result, nucleonic configurations based on the occupation of such hyper- and mega-intruder orbitals become yrast or near yrast at high angular momentum in the calculations. Two examples of such configurations are discussed below.

Note that these orbitals emerge two or three shells above the normal shell in which the Fermi level is located at normal deformation. As a consequence, these orbitals have substantially larger radius of the single-particle states than those located in the normal shell (see, for example, Table 1 in Ref. [16]). Moreover, because of extreme deformation there is a very strong $\Delta N = 2$ mixing in the structure of the single-particle wave functions (see Sec. 5.2.2 in Ref. [12]). The combination of these factors with the concentration of the matter of the $[NN0]1/2$ states in polar regions of nucleus leads to cluster-type giant proton halo in proton subsystem of rotational bands ^{14,18}Ne (see Fig. 4). It consist of high density prolate central cluster and low density ($\rho_\pi \approx 0.01$ fm^{-3}) clusters centered at around $z \approx \pm 7$ fm. Note that ^{18}Ne is the last proton-bound nucleus at spin zero. In contrast, the rotational band in ^{14}Ne becomes proton bound at high spin (see Ref. [12]).

5 Conclusions

In summary, the most important features of the nodal structure of the densities of the single-particle states at extreme deformation and their impact on α-clusterization, the formation of exotic shapes, nuclear molecules and ellipsoidal shapes have been analyzed. It turns out that the appearance of many exotic shapes in nuclear chart as a function of particle number can be inferred from combined analysis of typical pattern of single-particle densities and the evolution of the single-particle states in the Nilsson diagram with deformation and particle number. Such analysis allows to predict the existence of nuclear configurations with specific shape or cluster properties. For example, it indicates that only the lowest in energy two-fold degenerate deformed state of a given N-shell can contribute to the formation of the linear chain α cluster structures. Although such an analysis may look schematic, its validity is confirmed by a detailed fully self-consistent cranked relativistic mean field calculations presented in Refs. [10–12]. Note that collective rotation acts as a tool to bring exotic shapes of interest from high excitation energies at zero spin down to the yrast line at high spin.

References

[1] J.P. Ebran, E. Khan, T. Nikšić, D. Vretenar, Nature **487**, 341 (2012).
[2] M. Freer, H. Horiuchi, Y. Kanada-En'yo, D. Lee, U.G. Meißner, Rev. Mod. Phys. **90**, 035004 (2018).
[3] J. Han, Y. Ye, J. Lou, X. Yang, Q. Li, Z. Yang, Y. Yang, J. Wang, J. Xu, Y. Ge et al., Comm. Phys. **6**, 220 (2023).
[4] T. Otsuka, T. Abe, T. Yoshida, Y. Tsunoda, N. Shimizu, N. Itagaki, Y. Utsuno, J. Vary, P. Maris, H. Ueno, Nat. Comm. **12**, 2234 (2022).
[5] J.L. Egido, L.M. Robledo, Nucl. Phys. A **738**, 31 (2004).
[6] P. Arumugam, B.K. Sharma, S.K. Patra, R.K. Gupta, Phys. Rev. C **71**, 064308 (2005).
[7] P.G. Reinhard, J.A. Maruhn, A.S. Umar, V.E. Oberacker, Phys. Rev. C **83**, 034312 (2011).
[8] J.P. Ebran, E. Khan, T. Nikšić, D. Vretenar, Phys. Rev. C **90**, 054329 (2014).
[9] J.M. Yao, N. Itagaki, J. Meng, Phys. Rev. C **90**, 054307 (2014).
[10] D. Ray, A.V. Afanasjev, Phys. Rev. C **94**, 014310 (2016).
[11] A.V. Afanasjev, H. Abusara, Phys. Rev. C **97**, 024329 (2018).
[12] A.V. Afanasjev, S. Teeti, A. Taninah, Phys. Scripta **99**, 065313 (2024).
[13] J.M. Cavedon, B. Frois, D. Goutte, M. Huet, P. Leconte, C.N. Papanicolas, X.H. Phan, S.K. Platchkov, S. Williamson, W. Boeglin et al., Phys. Rev. Lett. **49**, 978 (1982).
[14] B. Frois, J.M. Cavedon, D. Goutte, M. Huet, P. Leconte, C.N. Papanicolas, X.H. Phan, S.K. Platchkov, S.E. Williamson, Nucl. Phys. **396**, 409 (1983).
[15] U.C. Perera, A.V. Afanasjev, Phys. Rev. C **106**, 024321 (2022).
[16] U.C. Perera, A.V. Afanasjev, Phys. Rev. C **107**, 064321 (2023).
[17] P.W. Zhao, N. Itagaki, J. Meng, Phys. Rev. Lett. **115**, 022501 (2015).
[18] S.E. Agbemava, A.V. Afanasjev, D. Ray, P. Ring, Phys. Rev. C **89**, 054320 (2014).
[19] G.A. Lalazissis, S. Karatzikos, R. Fossion, D.P. Arteaga, A.V. Afanasjev, P. Ring, Phys. Lett. **B671**, 36 (2009).
[20] A.V. Afanasjev, H. Abusara, Phys. Rev. C **82**, 034329 (2010).
[21] W. von Oertzen, M. Freer, Y. Kanada-En'yo, Phys. Rep. **432**, 43 (2006).
[22] T. Ichikawa, J.A. Maruhn, N. Itagaki, S. Ohkubo, Phys. Rev. Lett. **107**, 112501 (2011).

[23] E. Ideguchi, D.G. Sarantites, W. Reviol, A.V. Afanasjev, M. Devlin, C. Baktash, R.V.F. Janssens, D. Rudolph, A. Axelsson, M.P. Carpenter et al., Phys. Rev. Lett. **87**, 222501 (2001).

[24] P. Ring, P. Schuck, *The Nuclear Many-Body Problem* (Springer-Verlag, Berlin) (1980).

[25] M.J.A. de Voigt, J. Dudek, Z. Szymański, Rev. Mod. Phys. **55**, 949 (1983).

[26] Y.R. Shimizu, J.D. Garrett, R.A. Broglia, M. Gallardo, E. Vigezzi, Rev. Mod. Phys. **61**, 131 (1989).

[27] S. Karatzikos, A.V. Afanasjev, G.A. Lalazissis, P. Ring, Phys. Lett. B **689**, 72 (2010).